Developmental Biology 477 (2021) 145–154

Contents lists available at ScienceDirect

Developmental Biology

journal homepage: www.elsevier.com/locate/developmentalbiology

Single cell transcriptomic analysis of external genitalia reveals complex and sexually dimorphic cell populations in the early genital tubercle

Brooke A. Armfield [a], Martin J. Cohn [a,b,*]

[a] Department of Molecular Genetics and Microbiology, UF Genetics Institute, University of Florida, Gainesville, FL, 32610, USA
[b] Department of Biology, University of Florida, Gainesville, FL, 32611, USA

ARTICLE INFO

Keywords:
External genitalia
Genital tubercle
Mouse embryo
Urethra
Single cell sequencing

ABSTRACT

External genital organs are among the most recognizable sexually dimorphic characters. The penis and clitoris develop from the embryonic genital tubercle, an outgrowth at the anterior margin of the cloaca that undergoes an extensive period of development in male and female embryos prior to the onset of sexual differentiation. In mice, differentiation into the penis and clitoris begins around embryonic day (E)15.5. Current knowledge of cell types that comprise the genital tubercle is limited to a few studies that have fate mapped derivatives of endoderm, mesoderm, and ectoderm. Here we use single cell transcriptomics to characterize the cell populations in the genital tubercles of male and female mouse embryos at E14.5, approximately 24 h before the onset of sexual differentiation, and we present the first comprehensive atlas of single-cell gene expression during external genital development. Clustering analyses and annotation using marker genes shows 19 distinct cell populations in E14.5 genital tubercles. Mapping of cell clusters to anatomical locations using *in situ* gene expression patterns revealed granularity of cellular specializations and positional identities. Although E14.5 precedes sexually dimorphic morphogenesis of the genital tubercle, comparative analysis of males and females identified sexual dimorphisms at the single cell level, including male-specific cell clusters with transcriptional signatures of smooth muscle and bone progenitors, both of which are known to be sexually dimorphic in adult genitalia, as well as immune cells. These results provide a new resource for classification of external genital cell types based on gene expression profiles and reveal sex-specific cellular specializations in the early genital tubercle.

1. Introduction

The distinctive morphologies of male and female external genitalia result from sexual differentiation of the embryonic genital tubercle. Early outgrowth and patterning of the genital tubercle are controlled by conserved gene regulatory networks that are expressed in similar patterns in males and females (Haller and Ma, 2019; Hashimoto et al., 2019; Lin et al., 2013). Sexual differentiation of the genital tubercle is a relatively late event, beginning around embryonic day (E)15.5 in mice (Seifert et al., 2008), and is influenced by sex hormones produced by the testes and the ovaries. Developmental genetic and endocrinological studies have led to a two-phase model of external genital development in which outgrowth and patterning of the sexually indeterminate genital tubercle occur during an early, hormone-independent phase, and sexual differentiation of the penis and clitoris occurs during a hormone-dependent phase.

1.1. Early development of external genitalia

The progenitor cells that give rise to external genitalia originate from the lateral-most lateral plate mesoderm at the level of the hindlimb fields (Herrera and Cohn, 2014; Tschopp et al., 2014). The left and right external genital fields are brought together at the ventral midline of the embryo during closure of the posterior body wall (Herrera and Cohn, 2014). In all amniotes examined to date, outgrowth of external genitalia begins with the emergence of paired genital swellings on either side of the cloacal membrane (Gredler et al., 2014, 2015a, 2015b; Herrera et al., 2015; Larkins and Cohn, 2015; Leal and Cohn, 2015; Sanger et al., 2015). In the mouse, the paired genital swellings appear around E10.5, and the swellings merge to form a single tubercle by E11 (Perriton et al., 2002). The endodermally derived epithelium that lines the ventral wall of the cloaca extends into the genital tubercle and forms a bilaminar urethral plate, which later tubularizes to form the urethra in males (Hynes and Fraher, 2004a). As distal outgrowth of the genital tubercle continues, an

* Corresponding author. Department of Molecular Genetics and Microbiology, UF Genetics Institute, University of Florida, Gainesville, FL, 32610, USA.
E-mail addresses: barmfield@ufl.edu (B.A. Armfield), mjcohn@ufl.edu (M.J. Cohn).

https://doi.org/10.1016/j.ydbio.2021.05.014
Received 24 March 2021; Received in revised form 13 May 2021; Accepted 17 May 2021
Available online 24 May 2021

additional pair of swellings, known as the preputial swellings, emerges at its base and surrounds the tubercle dorsally and ventrally to form the prepuce (or foreskin). At E14.5 a small ventral opening, known as the urethral duct or proximal urethral opening (PUO), appears at the base of the genital tubercle, near the position where the urorectal septum contacts the cloacal membrane (Georgas et al., 2015; Perriton et al., 2002). These early events in external genital development are indistinguishable in males and females, and, as such, are considered to be hormone-independent (Suzuki et al., 2002).

1.2. Sexual differentiation of the penis and clitoris

Sex differences begin to appear in the mouse genital tubercle at E15.5 (Seifert et al., 2008; Suzuki et al., 2002; Zheng et al., 2015), when a mesenchymal extension of the urorectal septum extends into the genital tubercle of males, separating the urethral plate into the definitive urethra on the dorsal side and the urethral seam, or raphe, on the ventral side (Seifert et al., 2008). In females, the urorectal septum does not extend into the genital tubercle, and, consequently, the urethral plate remains contiguous with the ventral skin of the clitoris. Around the same stage, the urethral duct/PUO closes in males but persists to form the vulval opening in females (Kurita, 2010). Mesenchyme of the genital tubercle condenses around the urethral epithelium, where it differentiates into smooth muscle and spongy connective tissue (corpus cavernosum urethrae, the mouse homolog of human corpus spongiosum) (Hynes and Fraher, 2004b; Murakami, 1987; Phillips et al., 2015). Dorsal to the urethra, two mesenchymal condensations form the anlage of the erectile bodies, the corpus cavernosum glandis (Perriton et al., 2002). These spongy erectile tissues become highly vascularized and are surrounded by a fibrous sheath (tunica albuginea) in the penis and the clitoris. Outgrowth of the penis and tissue differentiation within the penis and the clitoris continue until approximately postnatal day (P) 25 (Phillips et al., 2015).

Androgens (testosterone and dihydrotestosterone) and estrogen are the primary sex hormones that direct sexual differentiation of the genital tubercle to form a penis or a clitoris, respectively (Glucksmann et al., 1976; Guillette et al., 1996; Hutson et al., 2014; Murakami, 1987; Stewart et al., 2018; Zheng et al., 2015). Mutations in genes that encode the androgen receptor (*Ar*/AR) and estrogen receptor alpha (*Esr1*/ERα) have opposite effects on external genital development; males with *Ar* mutations have androgen insensitivity and develop female-typical external genitalia, whereas females with *Esr1* mutations develop an elongated clitoris containing male-typical skeletal features (Goldstein and Wilson, 1975; Lyon and Hawkes, 1970; Yang et al., 2010).

1.3. Congenital anomalies of external genitalia

Congenital anomalies of external genitalia are among the most prevalent birth defects in humans, affecting approximately 1:120 newborn males (Nelson et al., 2005; Springer et al., 2016). Most congenital penile variations (CPVs) reflect developmental disruptions that occur during sexual differentiation of the genital tubercle, but the underlying causes are largely unknown. Aside from syndromic differences in sex development (DSDs), which result from mutations in sex steroid signaling pathways, most congenital penile anomalies are of unknown etiology. CPVs such as penile hypoplasia (severely reduced outgrowth, or micropenis) and hypospadias (a failure of urethral tube formation) can be viewed as reduction or loss of male-typical morphology, and severely affected individuals can have ambiguous genitalia. Hypospadias is the most common CPV and is characterized by ectopic urethral opening(s) on the underside of the glans, along the penile shaft, in the scrotum, or even in perineum (Nelson et al., 2005; Springer et al., 2016). In severe hypospadias, the urethra can be cleft along the entire ventral side of the phallus, causing it to look more like a clitoris and vulva than a penis. Surgical intervention is usually required to restore urologic and sexual function, and even mild forms of hypospadias can require multiple surgeries and involve post-operative complications (Andersson et al., 2020; Mohammed et al., 2020; Ru et al., 2021; Taneli et al., 2021). Surgical correction is fraught with challenges, as hypospadias generally is associated with significant deficiency of the tissues necessary to reconstruct a urethra, particularly the corpus spongiosum and urethral plate. Thus, methods to isolate, culture, and/or stimulate growth of specific penile tissues, such as corpus spongiosum, are critically needed to improve outcomes of surgical interventions. However, at present, the lack of knowledge needed to identify the cell and tissue types in external genital organs is a major obstacle.

Identification of the cell types that comprise the genital tubercle, the genes that specify cell type identities and regulate their differentiation, and the cellular and molecular differences between male and female external genitalia is needed to improve our understanding of the mechanisms of external genital development and the causes of congenital anomalies. Here we report on an unbiased single-cell RNA sequencing analysis of the mouse genital tubercle and we map single cell transcriptomic data to an anatomical context using *in situ* patterns of gene expression in mouse embryos.

2. Results

2.1. Cellular diversity in the developing genital tubercle

To determine the cellular diversity in male and female genital tubercles immediately before the onset of sexual differentiation, we performed single-cell RNA sequencing (scRNA-seq) of E14.5 mouse genital tubercles that were PCR-genotyped to verify chromosomal sex (Fig. 1A). Single-sex pools of genital tubercle (GT) cells were dissociated, screened for viability, counted, and loaded separately into a 10x Genomics Chromium instrument. Single cell libraries were sequenced to a depth of approximately 15,000 mean reads per cell using an Illumina NextSeq 500/550. Transcriptional profiles of 40,945 cells passed initial quality control screening with an average read depth of 2039 median genes per cell. After second-stage quality control and filtering using the Seurat R package (Butler et al., 2018; Satija et al., 2015), 35,619 cells were retained for analysis (see materials and methods for additional details).

We identified 19 distinct clusters of GT cells based on expression of highly variable genes across the population using an unsupervised cluster analysis of de-multiplexed male and female single cell transcriptomes (Fig. 1B, Supplementary Table 1). Clusters were visualized using 'uniform manifold approximation and projection' (UMAP) following data dimensionality reduction by principal-component analysis (PCA). Nine clusters were assigned preliminary cell type identities based on gene ontology (GO) analysis and a screen of transcriptional profiles for known marker genes (Fig. 1C; Table 1). The 9 clusters included 1 epithelial cell cluster (C11), 1 endothelial cell cluster (C12), 2 immune cell clusters (C18 and C19), 1 neural cell cluster (C15), 2 blood cell clusters (C16 and C17), and 2 clusters of muscle cells (C13, C14), which we resolved as 1 smooth muscle cluster (C13) and 1 striated/skeletal muscle cell cluster (C14). The remaining 10 clusters, which were less distinct from one another, were driven by expression of "tissue development-morphogenesis" gene functions and were classified as mesenchymal cells (Fig. 1C, Table 1; see below). Resolution of these 19 distinct cell clusters shows complex cell type specialization in the sexually undifferentiated genital tubercle.

2.2. Mesenchymal cell clusters reveal progenitors of morphological structures of the penis and clitoris

To refine the 10 cell clusters that were classified as "mesenchyme", we performed a re-clustering analysis of only those cells. We identified 8 subclusters of mesenchymal cells, although these appear to reflect heterogeneity within the mesenchymal cell population rather than distinct cell types (Fig. 2A, Supplementary Table 2). We then used the top

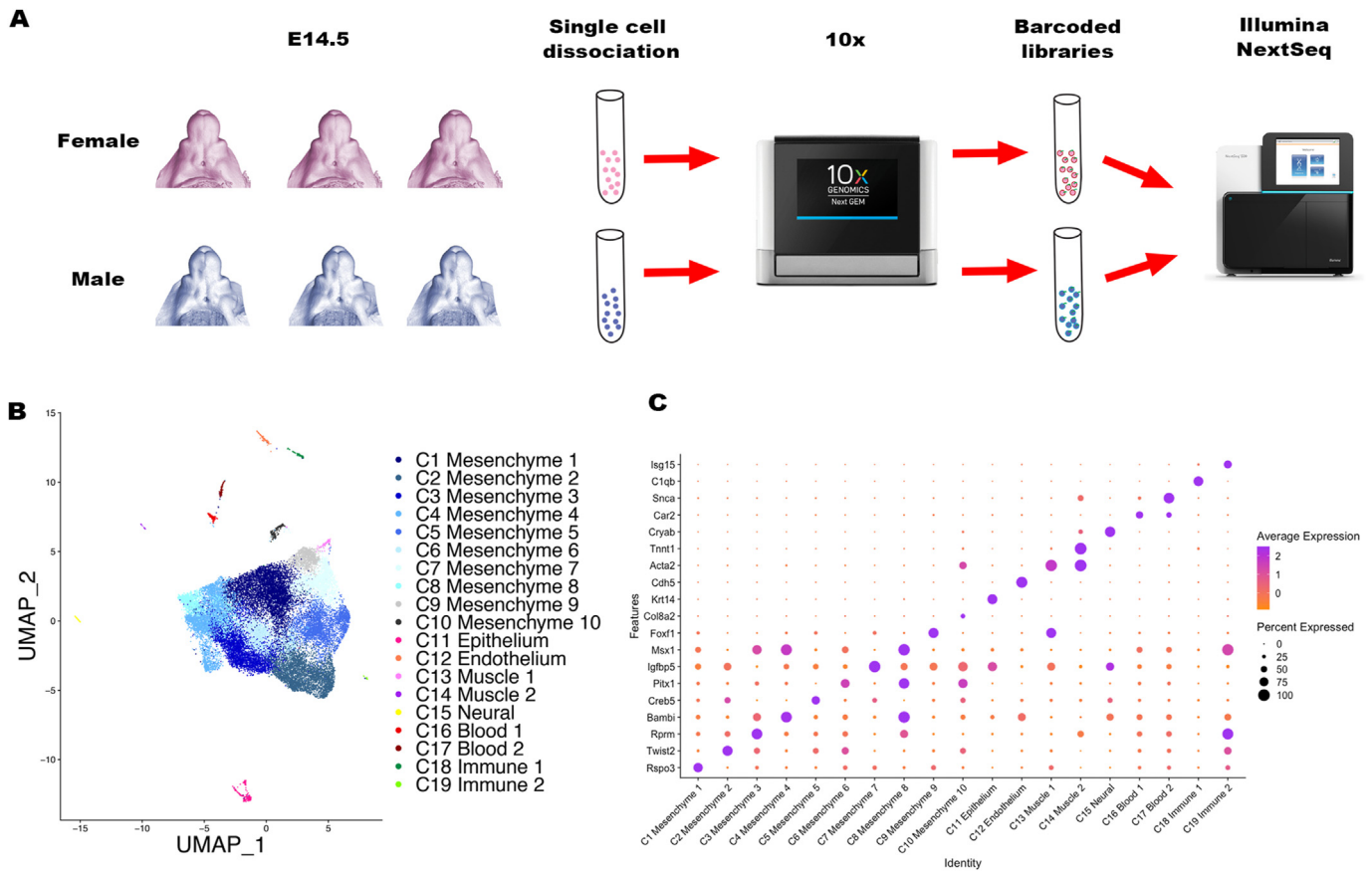

Fig. 1. Single cell analysis of E14.5 mouse genital tubercles reveals 19 distinct cell clusters. A. Diagrammatic representation of the workflow showing genital tubercles of 3 male and 3 female mouse embryos at E14.5, single cell dissociation, and the downstream cell preparation and sequencing. **B.** UMAP plot of male and female genital tubercle cells showing 19 distinct clusters by data dimensional reduction. Cluster and cell type identities are indicated by GO annotation. **C.** Dot plot of marker genes representing different clusters. Color scale indicates average expression (normalized and scaled) and the size of the dots indicates the percentage of cells expressing the gene.

Table 1
Marker genes for each cluster.

ID	Cluster	Top differentially expressed genes
C1	Mesenchyme 1	*Rspo3, Zfhx4, Zfhx3, Lmo4, Klf4*
C2	Mesenchyme 2	*Twist2, Igf1, Meg3, Shox2, Ezr*
C3	Mesenchyme 3	*Rprm, a, Cxcl14, Tac1, Msx1*
C4	Mesenchyme 4	*Bambi, Dlx5, Msx1, Ptn, Msx2*
C5	Mesenchyme 5	*Nefm, Creb5, Nefl, Meis1, Epha4*
C6	Mesenchyme 6	*Vim, Pitx1, Cdo1, Flrt2, Ntm*
C7	Mesenchyme 7	*Igfbp5, Sfrp2, Igfbp2, Meis2, H19*
C8	Mesenchyme 8	*Bambi, Pitx1, Msx1, Cxcl14, Msx2*
C9	Mesenchyme 9	*Foxf1, Foxp2, Aldh1a2, Tcf21, Gucy1a1*
C10	Mesenchyme 10	*Asb4, Col8a2, Tagln, Col9a3, Acta2*
C11	Epithelium	*Krt14, Krt5, Krt15, Perp, Sfn*
C12	Endothelium	*Gng11, Cdh5, Emcn, Egfl7, Col18a1*
C13	Muscle 1	*Acta2, Tcf21, Actg2, Myocd, Cnn1*
C14	Muscle 2	*Actc1, Tnnt1, Mylpf, Myog*
C15	Neural	*Ednrb, Cryab, Plp1, Foxd3, Phactr1*
C16	Blood 1	*Hbb-bh1, Car2, Alas2, Hsd3b6, Pdzk1ip1*
C17	Blood 2	*Snca, Alas2, Alc25a37, Gypa, Pnpo*
C18	Immune 1	*C1qb, Fcer1g, Pf4, Tyrobp, C1qc*
C19	Immune 2	*Isg15, Usp18, Ifit1, Rtp4, Ifi44*

differentially expressed (DE) genes in the transcriptomes of each cluster to map cells to anatomical domains within the genital tubercle and found that several cell clusters show distinct patterns of spatial localization (Fig. 2A–C). Analysis of the *in situ* expression patterns of highly differentially expressed genes in E14.5 genital tubercles revealed that 6 clusters of cells map to positions that correspond to progenitors of specific anatomical structures, including the corpus cavernosum (cc) glandis, cc urethrae (corpus spongiosum), urethral duct/(PUO), dorsal aspect of the genital tubercle, glans, and prepuce (Fig. 2C). Two clusters could not be resolved to specific regions based on gene expression patterns, and, therefore, retained the general classification of mesenchymal cells.

Comparisons of transcriptional signatures across all mesenchymal cell clusters showed that while some DE genes showed qualitative differences in expression, and, as such, were markers of single clusters, many DE genes are expressed in more than one cluster, although at quantitatively different levels. For example, *Vim* is a top DE gene in the dorsal tubercle cluster, and although *Vim* is expressed in 7 mesenchymal clusters, dorsal tubercle is characterized by the highest expression in the greatest number of cells (Fig. 2D). On the other hand, genes like *Foxf1*, which is expressed almost exclusively within the cc urethrae, were determined to be true marker genes for specific cell clusters (Fig. 2E). Thus, both presence/absence and quantitative thresholds of gene expression can be used to resolve cell identities in the GT. The finding that subsets of genes within each cluster's transcriptional signature are expressed across multiple clusters, albeit at different levels, is consistent with the common lineage of genital tubercle mesenchyme and shows that cells within the genital tubercle are still undergoing differentiation at E14.5.

Genetic studies in mice and humans have identified a number of transcription factors with key roles in external genital development and suggest that the embryonic genital tubercle may be patterned by regionalized expression of transcription factors (Gredler et al., 2020; Matsumaru et al., 2014; Su et al., 2019; Suzuki et al., 2008; Wang et al., 2013). Therefore, we investigated the spatial distributions of DE transcription factors in mesenchymal cells of the genital tubercle. We identified 106 transcription factors that exhibited an average log2 fold

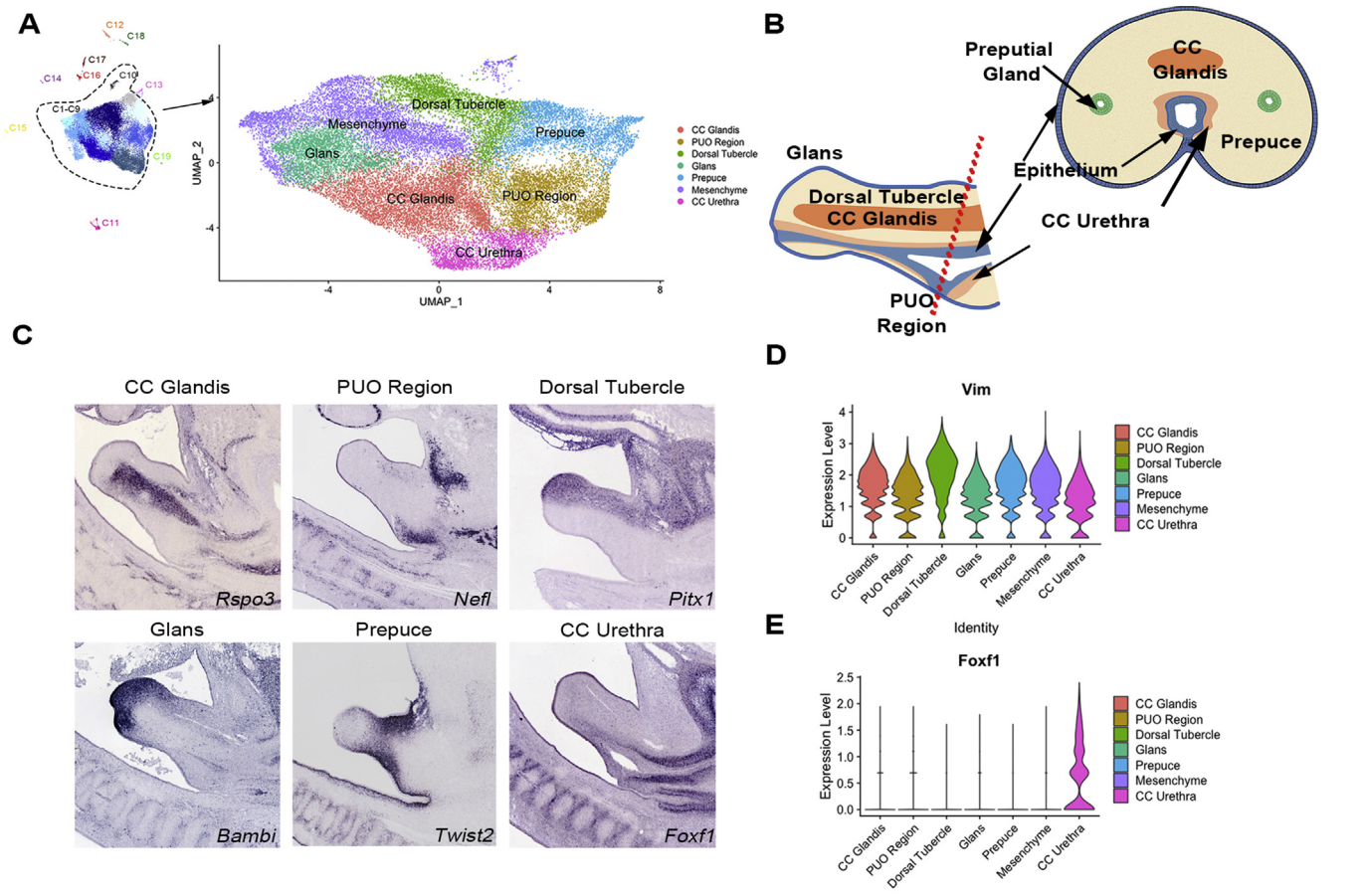

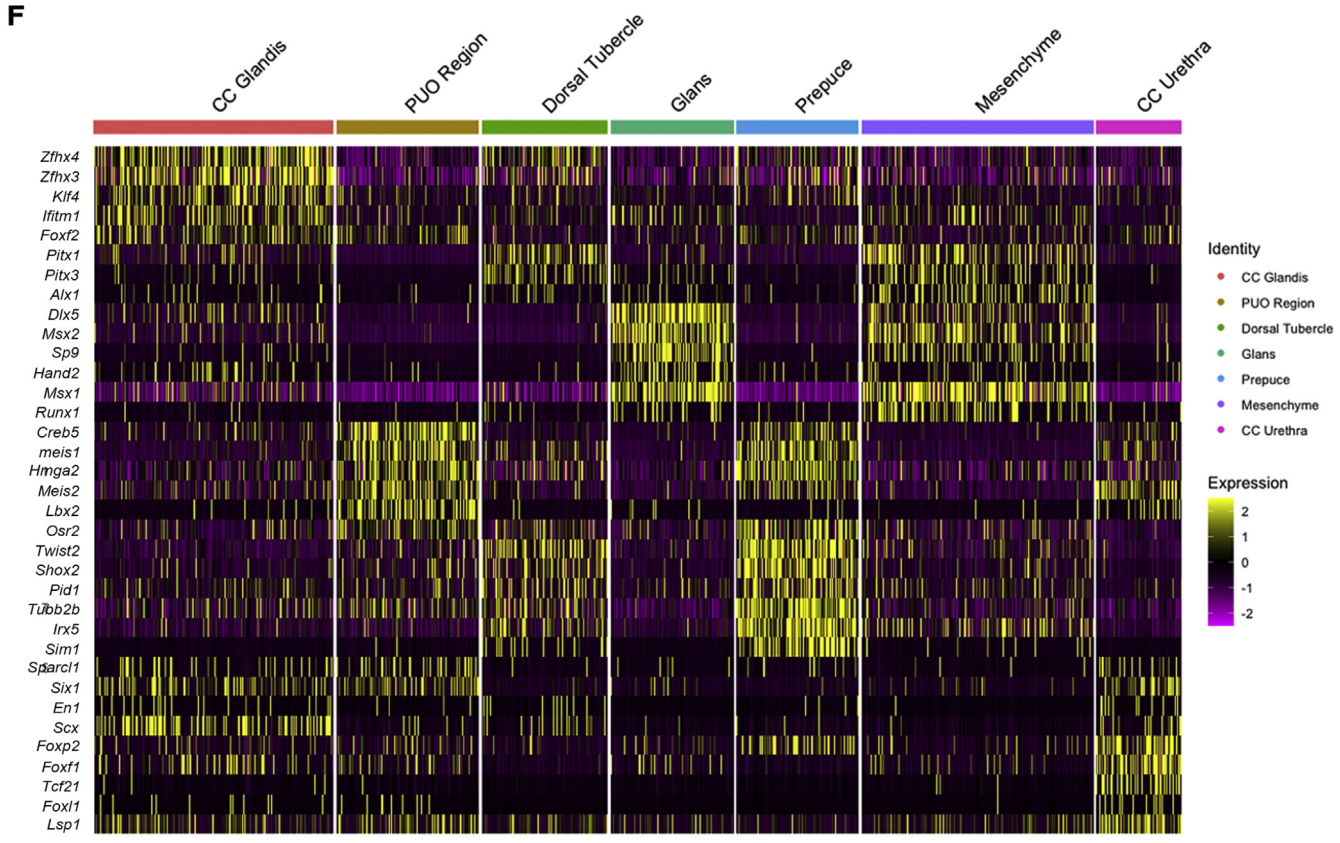

(caption on next page)

Fig. 2. Mesenchymal cell clusters correspond to specific anatomical regions of the genital tubercle. A. Mesenchymal cells re-clustered to identify specific cell identities. Cluster identities were assigned based on *in situ* gene expression patterns. **B**. Schematic diagram of the six morphological regions identified in the cell cluster analysis. **C**. *In situ* hybridization results from GenePaint showing the spatial expression patterns of genes from the 6 morphological regions shown in (B). GenePaint set ID numbers are as follows: C3591.2.4.B (*Rspo3)*, C2673.4.3.D (*Nefl), C2854.3.4.C* (*Pitx1*), *C2679.4.4.B* (*Bambi*), *G0435.1.3.C* (*Twist2*), C4026.1.4.B (*Foxf1*). Additional sections and interactive magnification can be accessed on the GenePaint website (gp3.mpg.de). **D**. *Vim* expression across clusters is shown as an example of a gene that is highly expressed in the dorsal genital tubercle but also is found throughout the mesenchymal cells. **E**. *Foxf1* expression across clusters is shown as an example of a gene expressed almost exclusively in one cluster. **F**. Heatmap of transcription factors expressed across mesenchymal cell clusters.

change of 0.25 in one cell cluster compared to all others (Supplementary Table 3). Hierarchical clustering analysis of the top 5 DE genes in each cell cluster highlighted a number of transcriptional signatures that associate with specific morphological features in the genital tubercle (Fig. 2F). For example, the erectile tissues – cc glandis and cc urethrae – contain clusters of cells with similar transcription factors, such as *Six1, Sparcl1*, *En1*, *Scx*, *Foxp2*, *Foxf1*, and *Lsp1*. This shared expression profile may reflect (and potentially control) the similarities in the tissue types found within these structures. Interestingly, the cluster we designated as indistinct mesenchyme has an expression pattern similar to cc glandis, dorsal tubercle, and glans clusters, raising the possibility that these clusters may contain cells from these same anatomical regions but at less advanced stages of differentiation. Alternatively, these clusters could consist of cell types that are found throughout the body of the genital tubercle but are excluded from domains such as the ventral tubercle and the prepuce.

2.3. Epithelial cell clustering suggests that urethral epithelium is homogeneous at E14.5

Our initial analysis produced a single cluster of cells associated with epithelial cell types; however, the genital tubercle contains several epithelial tissues, including the genital skin and preputial glands, which are derived from surface ectoderm, and the urethral plate epithelium, which is derived from endoderm (Figs. 1B and 3A). To refine the identity of the epithelial cell cluster, we performed a re-clustering analysis of the epithelial cells and identified 4 distinct subclusters (Fig. 3B, Supplementary Table 4). Our analytical pipeline identified a single subcluster of urethral epithelial cells, which expressed urethral plate marker genes such as *Shh*, *Upk3bl*, *Foxa1*, and *Foxa2* (Fig. 3C and D). Although *Shh* is found in the urethral plate and in preputial glands at E14.5, preputial gland identity could be excluded by the presence of *Upk3bl*, *Foxa1,* and *Foxa2,* which are known markers of the developing urethra (Gandhi et al., 2013; Gredler et al., 2020) (Fig. 3E). Further subclustering of epithelial cells yielded no further separation regardless of the parameters used, although cluster 1 also contains *Shh*-expressing cells and, therefore, it could contain ectodermal cells of the preputial gland (Fig. 3D).

Urethral epithelial cells share many properties, including lineage, with bladder epithelium. The developing urothelium of the embryonic bladder consists of several distinct cell types, including basal, intermediate, progenitor, and superficial cells, which can be identified between E13.5 and E14.5 by the presence/absence of four marker genes (*Foxa2*, *Trp63*, *Upk*, and *Krt 5*). All 4 marker genes were present throughout the urethral epithelial cluster (Fig. 3F), but not in the specific combinations that distinguish the cell layers of the urothelium. These results suggest that urethral epithelium at E14.5 is relatively homogeneous.

2.4. Cells of the undifferentiated genital tubercle show molecular sexual dimorphisms

The clustering patterns of mesenchymal cells of the genital tubercle at E14.5 led us to investigate whether some cells have already begun to express markers of adult cell types and whether male and female genital tubercle cells have distinct molecular profiles at this stage. UMAP plots revealed one cluster (C10) that appeared to have mostly male cells (Fig. 4A). Quantitative comparison of male and female cells across all clusters confirmed that cluster 10, which was categorized as undifferentiated mesenchymal cells, is composed predominantly of male cells (Fig. 4B). We then reclustered only the mesenchymal cells to determine if this male-centric cluster could be further differentiated from the other mesenchymal cells. Again, a distinct cluster of male cells categorized as undifferentiated mesenchyme was recovered (Fig. 4C). We then used a differential expression analysis, DEseq2, to identify genes that were significantly different between male and female cells within that cluster of cells (Supplementary Table 5). Within the male-biased cluster, strongly dimorphic expression patterns were detected for a number of genes, including *Acta2*, *Tagln*, *Ptn*, *Cdkn1c*, *Sparc,* and *Lum*, all of which are upregulated in males compared to females (Fig. 4D). The *in situ* expression patterns of these genes map to different regions of the genital tubercle, and they are known to mark a variety of cell types in other organs. For example, *Acta2* and *Tagln* are both associated with smooth muscle (Chakraborty et al., 2019; Gomez et al., 2015). *Ptn* regulates cell proliferation, cell survival, cell differentiation and cell migration in neurons and bone (Wang et al., 2020). *Cdkn1c* is an imprinted gene that is a negative regulator of cell proliferation. Mutations in *Cdkn1c* result in Beckwith-Wiedemann syndrome, which includes ambiguous genitalia (Creff and Besson, 2020). *Sparc* encodes a protein that is required for calcification of collagen in bone (Rosset and Bradshaw, 2016). *Lum* also is involved in regulating collagen fibrillogenesis (Chen and Birk, 2013). Overall, the genes that differentiate the male cell clusters are associated with smooth muscle and bone formation, both of which are known to be sexually dimorphic in the adult genitalia.

Sequence analysis of the top DE genes in male-specific cell clusters identified a number of genes (e.g., *Sparc, Ptn, Acta2*) that contain consensus sequences for AR binding, known as androgen response elements (AREs). AREs consist of two hexameric half-sites separated by a 3-nucleotide spacer, and the half sites can be arranged as either inverted repeats in the classical ARE or as direct repeats in the selective ARE (Denayer et al., 2010; Shaffer et al., 2004). Although biological activity of ARE sequences requires evidence of AR binding and functional assays, the results suggest that these mesenchymal cell clusters segregate due to expression of androgen-responsive genes. This is consistent with our previous finding that AR expression in genital tubercle mesenchyme is critical for differentiation of the penis and urethral tube (Zheng et al., 2015).

We also searched for sex differences in epithelial cells but found no significant difference in the number of male and female cells that contributed to epithelial cell clusters. However, analysis of androgen receptor (*Ar*) expression in epithelial cells revealed a striking sex difference; the number of male cells expressing *Ar* far exceeded the number of *Ar*-expressing female cells (Fig. 4F). Although this finding suggests a sex difference in androgen responsiveness of urethral cells at E14.5, in previous studies we demonstrated that AR expression in epithelial cells is not required for development of the penile urethra (Zheng et al., 2015).

3. Conclusions

In this study, we characterized 35,619 single-cell transcriptomes to produce the first comprehensive cellular atlas of the genital tubercle of male and female mouse embryos. These experiments were carried out on mouse embryos at E14.5, approximately 1 day before male and female external genital development begins to diverge; however, we identified multiple sexual dimorphisms at the single-cell level. Cluster analysis, including sequential subclustering, allowed the resolution of 22 cell populations, including 10 distinct populations of mesenchymal cells, 4 populations of epithelial cells, 2 populations each of blood cells, immune

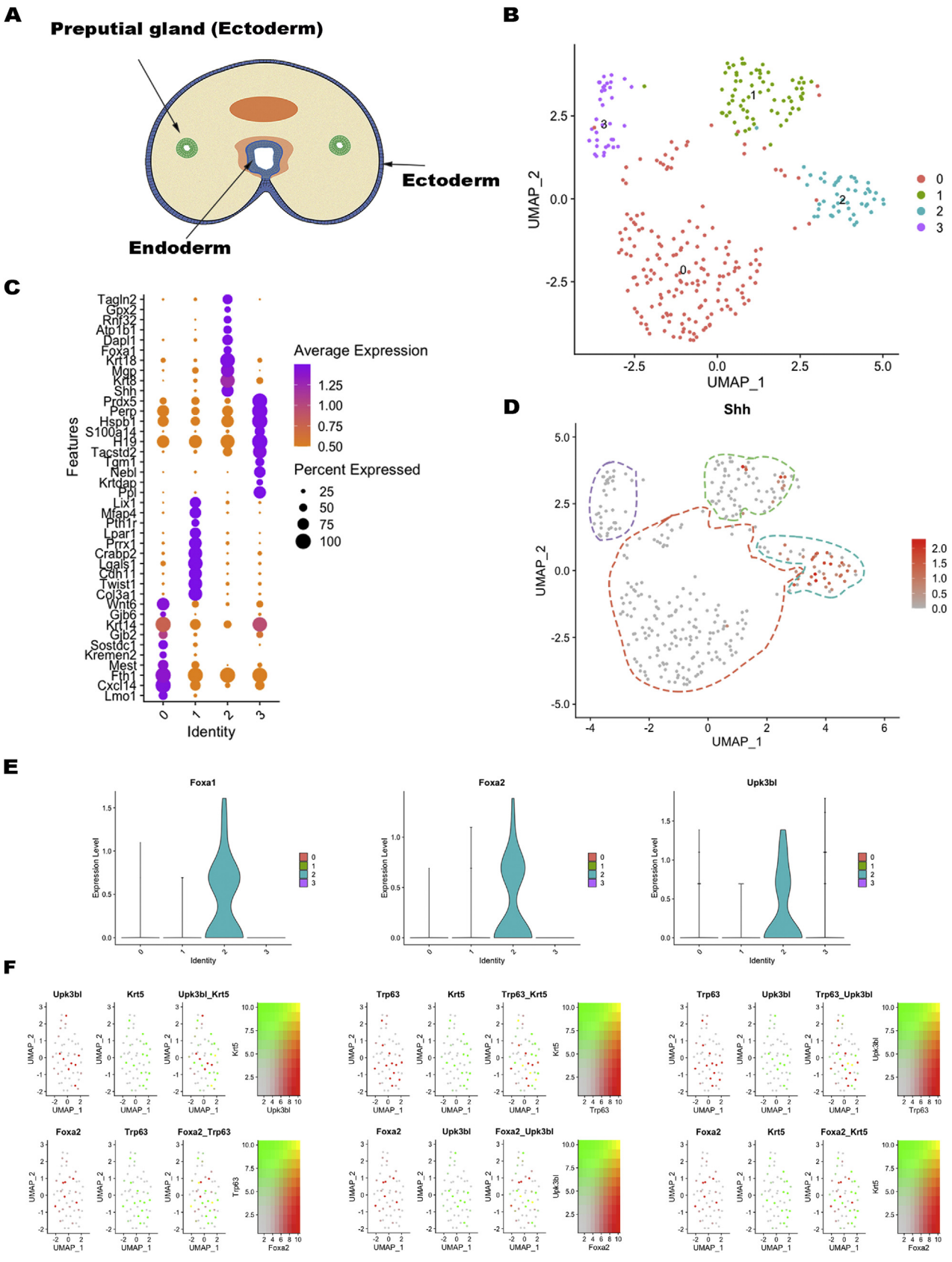

Fig. 3. Epithelial cell clusters reveal homogeneity in the undifferentiated genital tubercle. A. Schematic diagram of the different epithelial cell types within the genital tubercle. **B**. Epithelial cells reclustered to resolve cell cluster identities. **C.** Dot plot showing the top 10 differentially expressed genes for each epithelial cluster. **D.** Feature plot of epithelial cell clusters. *Shh*-expressing cells are shown in red. Clusters are pseudocolored to distinguish them from each other. Note the presence of *Shh*-expressing (red) cells in clusters 1 and 2. **E.** Violin plot showing expression of the urethral epithelial and urothelial markers *Foxa1*, *Foxa2*, and *Upk3bl* predominantly in cluster 2. **F.** Feature plots of different combinations of urothelial cell type markers in urethral epithelial cells.

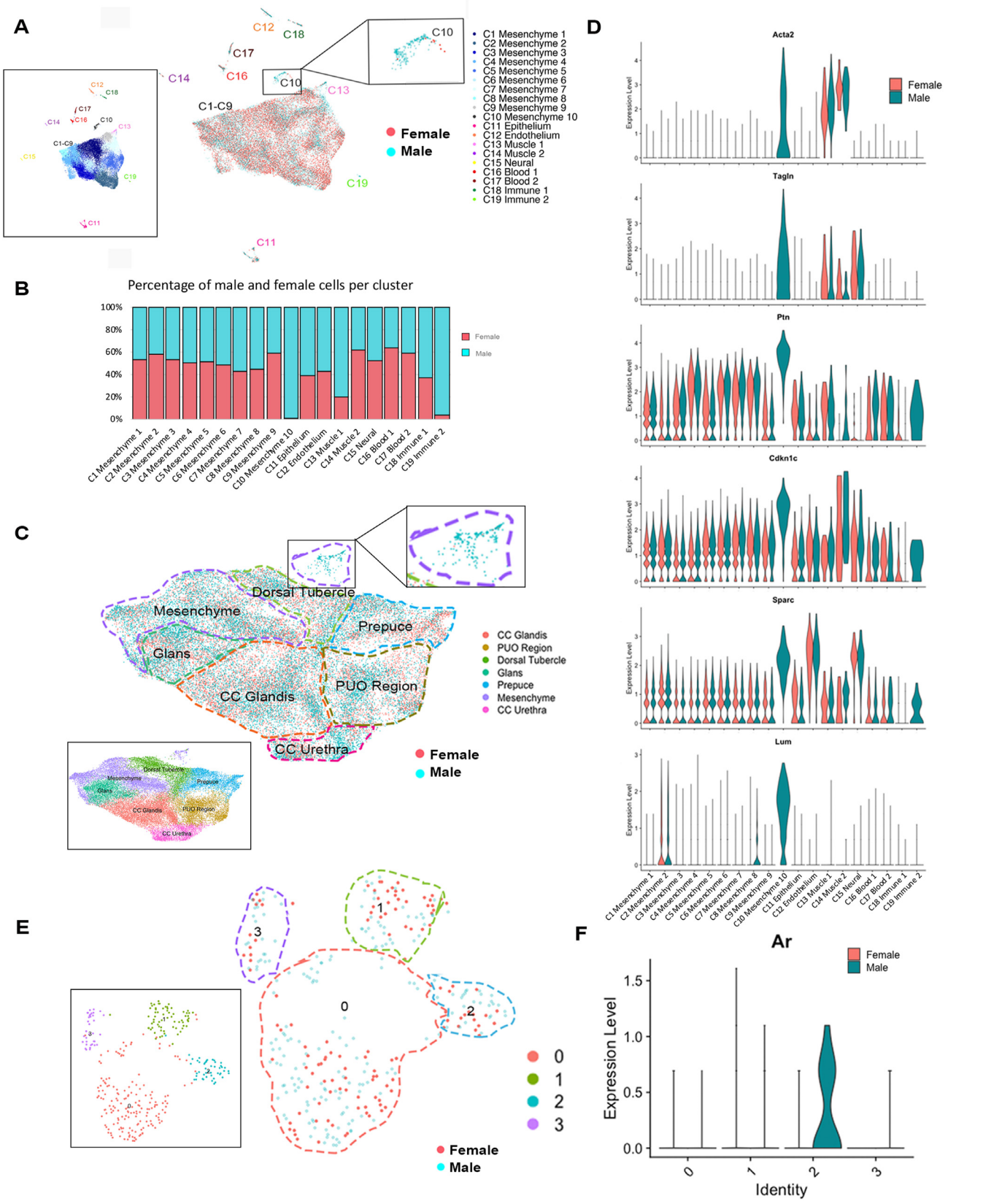

Fig. 4. Sexually dimorphic cell clusters in the E14.5 genital tubercle. A. UMAP of cells in the genital tubercle. Cell colors correspond to cell cluster identities (C1-C19) on the left and cell sex on the right. Cluster 10 (enlarged at right) consists predominantly of male cells. **B.** Graph showing percentage of male and female cells in each cluster. **C.** UMAP of mesenchymal cells by sex. Enlargement (right) shows cluster that constists predominately of male cells. **D**. Violin plots of select genes found to be differentially expressed in the male cells from cluster 10. **E**. UMAP of epithelial cells by sex. **F**. *Ar* expression in the epithelial cells.

cells, and muscle cells (1 smooth and 1 striated), and single populations of endothelial and neural cells. When we compared the top DE genes in mesenchymal cell clusters to *in situ* gene expression patterns, 6 of the 8 mesenchymal subclusters could be assigned to specific anatomical positions and tissue types, including the glans, the dorsal aspect of the genital tubercle, the urethral duct/PUO, the prepuce, and the corpora spongiosum and cavernosum. These results show that the transcriptomes of single cells reflect their molecular coordinates within the morphospace of the E14.5 genital tubercle and suggest that progenitors of key tissue types are established at this stage.

Given the relatively undifferentiated state of the genital tubercle at E14.5, the results of our subclustering analysis of mesenchymal cells raise a few possibilities regarding the nature of the cell clusters. One possibility is that the relative position of cells along the 3 major axes of the tubercle is the primary driver of clustering, and molecular markers of positional identity eclipse the heterogeneity of cell types or states within these spatial domains, in a manner similar to Hox gene expression domains in the limb bud or along the primary body axis. A variation on this interpretation is that the expression domains mark progenitor populations at a given position that are heterogeneous but at E14.5 are highly undifferentiated. Another possibility is that the dominant transcriptional profiles reflect cell types or cell states, and the *in situ* expression domains delineate homogeneous cell states or types at a given anatomical position. Generation of single-cell atlases in a fine-grained temporal series will allow discrimination among these possibilities.

In addition to the spatial domains described above, we identified two mesenchymal clusters that correspond to specific tissue types in the phallus, the cc urethrae (the mouse homolog of the corpus spongiosum) and the cc glandis. These results suggest that the progenitors of these specialized tissue types are specified relatively early in external genital development. In previous studies, we noted that mesenchymal cells in the proximal region of the E13.5 genital tubercle begin to aggregate in two domains that lie dorsal and lateral to the urethral plate (Perriton et al., 2002). By E14.5, these cells have formed the paired condensations of the cc glandis proximally, whereas the distal mesenchymal cells are just beginning to aggregate, suggesting that the erectile tissues develop in a proximal-to-distal direction. Our finding that genes expressed in mesenchymal cluster C1 localize to the cc condensations *in situ* suggests that this cluster contains progenitors of the paired corporal bodies. Given that differentiation of these erectile structures progresses from proximal-to-distal over time, we anticipate that progenitor cells of the distal cc should express genes reflective of their earlier state, and, therefore, they could lie outside of C1.

Development of the penile urethra in mice involves closure of the urethral duct/PUO at the base of the genital tubercle, whereas in females, this duct persists to form the vulval opening. Our analysis of genital tubercle mesenchyme identified a transcriptionally distinct subcluster of cells that map to the PUO. Given that only a small number of these genes have been implicated in urethral tube closure (Gredler et al., 2015c; Haraguchi et al., 2001; Morgan, 2003; Perriton et al., 2002), this dataset presents new opportunities for functional studies that should enhance our understanding of sexual differentiation of the urethra.

Comparison of stage-matched genital tubercles from male and female embryos at E14.5 revealed the presence of sexual dimorphisms at the single-cell level a full day before the onset of sexual differentiation of the phallus. Although most of the cell clusters in our analysis contained similar numbers of male and female cells, 3 cell clusters were sexually dimorphic; male cells comprised 99% of C10, 80% of C13, and 96% of C19. Key marker gene expression in the single-cell transcriptomes of these 3 clusters classified them as bone (C10), smooth muscle (C13) and immune (C19) cells (Fig. 4B; Table 1). Interestingly, the mature penis and clitoris show dramatic differences in both bone and smooth muscle tissues. Development of the penis bone (baculum or *os penis*) and clitoris bone (baubellum, or *os clitoridis*), both of which develop postnatally in mice, have long been thought to reflect differences in androgen signaling at late fetal and postnatal stages (Murakami, 1987; Murakami and Mizuno, 1986; Williams-Ashman and Reddi, 1991). During testis differentiation, Leydig cells begin synthesizing testosterone around E13 in the mouse (O'Shaughnessy et al., 1998). AR is activated when ligand binding in the cytoplasm triggers translocation of the receptor to the nucleus, where it binds DNA. At E13.5, male and female genital tubercles show similar cytoplasmic localization of AR, whereas at E15.5 (when sexual differentiation is initiated), AR protein is almost entirely nuclear in male genital tubercle mesenchyme but is undetectable in females (Zheng et al., 2015). Thus, at E14.5, when our scRNA-seq experiment was performed, mesenchymal cells are likely to experience different hormonal milieus in male and female genital tubercles. Our results suggest that the morphological differences between the baculum and baubellum, as well as the smooth muscle that surrounds the penile urethra, may be established in the progenitor cell pools in the early, sexually indeterminate genital tubercle.

We were intrigued by the sexually dimorphic nature of C19, one of two cell clusters enriched for expression of genes with "immune system process" GO classifications. Why would immune cells show a sex difference? Analysis of the combinations of DE genes in the "immune" clusters indicated that C18, which is non-dimorphic, shows the highest expression of macrophage markers, whereas C19 expressed markers of both the myeloid and the lymphoid hematopoietic cell lineages, including Isg15, Usp18, Ifit1, Rtp4, Ifi44. Hematopoietic stem cells (HSCs) have been shown to express a number of sex steroid receptors, including AR, and HSCs treated with androgen show increased proliferation (Mierzejewska et al., 2015). Thus, the dominance of C19 by male cells may reflect the early effect of gonadal androgens on the HSC lineage.

The mechanisms responsible for the sexual dimorphisms of cell clusters in the genital tubercle at E14.5 remain to be identified. As noted above, synthesis of gonadal sex hormones begins shortly before this stage, although hormone-independent mechanisms, such as sex-linked genes, could also have roles in establishing the cellular sexually dimorphisms of the genital tubercle. Indeed, genes residing on sex chromosomes have been implicated in sexually dimorphic morphologies, behaviors, and pathologies (Arnold, 2019). Sexually dimorphic epigenetic modifications also should be considered, as previous studies have identified sex differences in chromatin conformation and histone marks in cells of reproductive organs as early as E11.5 (Kawabata et al., 2019; Yang and Wilson, 2019). Taken together, the results presented here provide new resources for cell-specific genetic manipulation, open the possibility for the use of key anchor genes to target and/or isolate progenitors of critical tissue types isolated from the early genital tubercle, and provide a foundation for high-resolution analyses of signaling interactions, cellular dynamics, and cell lineage during normal and anomalous development of the external genitalia.

4. Materials and methods

4.1. Animals

Time-mated pregnant C57BL/6 mice were ordered from Charles River. Mice arrived 3 days before desired embryonic day and were housed in the animal facilities at the University of Florida. All animal experiments were conducted with approval of the University of Florida IACUC under protocol # 201803399.

4.2. Single cell dissociation, encapsulation, and library synthesis

Genital tubercles were harvested from pregnant female mice on embryonic day 14.5. Embryos were dissected in ice-cold Dulbecco's phosphate-buffered saline and tissue samples were collected for genotyping. Embryos were transferred to RPMI 1640 medium (Thermo Fisher Scientific, 11875093) and held on ice for $\leq$2 h while samples were genotyped to determine chromosomal sex. Three male and three female embryos were randomly selected from 2 litters, genital tubercles were dissected and sorted into 2 single-sex pools, and cells were dissociated

using collagenase XI (Sigma-Aldrich, C7657-25 MG). Collagenase XI (13 mg/ml stock) was first dissolved in TESCA buffer at 37 °C for 5 min and a working solution was prepared at 1.3 mg/ml in PBS containing 10% heat-inactivated fetal bovine serum. Genital tubercles were chopped into small pieces in 500 μl collagenase XI on ice and then transferred to 1.5 ml microcentrifuge tubes, which were agitated at 37 °C for 30 min and triturated using a glass Pasteur pipette every 5 min. After digestion, cells were centrifuged at 500 rpm for 5 min at 4 °C and then were resuspended in 100 μl of 1x PBS (magnesium- and calcium-free) with 0.04% bovine serum albumin, filtered through a 40 μm strainer (Flowmi Bel-Art H13680-0040), and the collection tube was placed on ice. Male and female samples were loaded separately into a 10x Genomics Chromium instrument for encapsulation, synthesis, and amplification of barcoded cDNAs (10X Next GEM Single Cell 3′ Gel Bead Kit v3.1). Libraries were prepared using the Chromium Single Cell Library kit V3 (10x Genomics) according to the manufacturer's instructions. After QC, Illumina libraries were sequenced on an Illumina NexSeq 500/550 using 2x150bp paired-end reads at a depth of approximately 15,000 mean reads per cell, which exceeds the depth required for robust, unbiased classification of cell types in heterogeneous tissues (Pollen et al., 2014).

4.3. Single-cell sequence analysis

Raw scRNA-seq data were demultiplexed into FASTQ files, aligned (mouse genome mm10), filtered, and UMIs and barcodes were counted using default settings in CellRanger (v3.1 10x Genomics). The samples consisted of 19,862 male cells with 2011 median reads per cell and 21,083 female cells with 2067 median reads per cell.

Male and female samples were merged and quality control was performed using Seurat (v3.2.3) (Satija et al., 2015) package in RStudio (v1.2.1335). To filter the data for possible doublets, free RNA, and cells with high mitochondrial gene expression, we set the parameters at nUMI count range of 1000–16,000, nfeatures to 1000–4000, log10genes per UMI greater than 0.80, a mitochondrial ratio of less than or equal to 0.15. and genes found to be expressed in greater than 10 cells. After filtering, 35,619 cells and 17,297 genes were retained for further analysis. We assigned a cell cycle score to each cell according to expression of G2/M and S phase markers (Tirosh et al., 2016) using the CellCycleScoring function in Seurat. We normalized and stabilized the variance of the filtered cells using the default parameters of the SCTransform function in Seurat and we removed confounding effects of cell cycle and mitochondrial genes. (Hafemeister and Satija 2019).

We then assessed the number of PCs to be included in downstream analysis by PCElbowPlot and PCHeatmap in Seurat. Our initial clustering of all cells was completed with 40 PCAs, as well as mesenchymal clustering. The subclustering of epithelial cells had 15 PCAs. For data dimension reduction visualization, we used UMAP and FindCluster in Seurat at a resolution of 0.6 to assign cell clusters for each protocol. Clusters identified to be associated with cell cycle were removed. The FindAllMarkers function in Seurat was used to identify the most significantly different genes expressed in each cluster when those genes were expressed at least in 25% cells within the cluster and with a fold change more than 0.25 (log scale).

To identify transcription factors that were enriched in each mesenchymal cluster, we first identified the most DE genes and then extracted the transcription factors and plotted them onto a heatmap using DoHeatmap. DE analysis was performed using the FindAllMarkers function in Seurat with the DEseq2 test (Love et al., 2014). Differentially expressed genes that were expressed at least in 25% of the cells within a cluster and with a fold change more than 0.25 (log scale) were considered to be marker genes.

4.4. In situ hybridization data

In situ gene expression patterns in the mouse genital tubercle were identified using the GenePaint digital atlas of gene expression, which is accessible at https://gp3.mpg.de/(Visel et al., 2004). GenePaint set ID numbers are provided for each gene in the legend to Fig. 2.

4.5. Sequence and gene ontology analyses

Sequences were examined for transcription factor binding sites using LASAGNA-Search 2.0 (Lee and Huang, 2013). Gene ontology (GO) analysis was conducted using PANTHER (v16) (Mi et al., 2013) to find significant biological processes associated with the top genes found in each cluster. These terms were used to aid in cell cluster characterization. The top 50 genes (or the maximum number of genes if there were less than 50 genes identifying the cluster) identified using FindAllMarkers were used for cluster classification analysis.

Data and code availability

The data described in this publication have been deposited in NCBI's Gene Expression Omnibus (Edgar et al., 2002) and are accessible through GEO Series accession number GSE175498 (https://www.ncbi.nlm.nih.gov/geo/query/acc.cgi?acc=GSE175498). Data Dissemination: To increase rigor, reproducibility, and transparency, raw sequencing files and other data generated as part of this study were deposited into the GUDMAP consortium database and are fully accessible at https://doi.org/10.25548/17-DSBR (Cohn, 2021).

Grant support

We gratefully acknowledge funding from National Institutes of Health grant number 1U01DK110812, which is part of the GenitoUrinary Development Molecular Anatomy Project (GUDMAP).

Acknowledgments

We thank Yanping Zhang and David Moraga (Gene Expression and Genotyping core and the NextGen DNA Sequencing core, respectively) of the Interdisciplinary Center for Biotechnology Research (ICBR) at the University of Florida for expert advice and assistance. We thank Emily Merton for technical support, Fred Souret (10X Genomics) for input on experimental design and analysis, and the GUDMAP Data Hub (Hongsuda Tangmunarunkit, Cristina Williams, Laura Pearlman, and Carl Kesselman) for assitance with data dissemination.

Appendix A. Supplementary data

Supplementary data to this article can be found online at https://doi.org/10.1016/j.ydbio.2021.05.014

References

Andersson, M., Sjöström, S., Doroszkiewicz, M., Örtqvist, L., Abrahamsson, K., Sillén, U., Holmdahl, G., 2020. Urological results and patient satisfaction in adolescents after surgery for proximal hypospadias in childhood. J. Pediatr. Urol. 16, 660.e661–660.e668.

Arnold, A.P., 2019. Rethinking sex determination of non-gonadal tissues. Curr. Top. Dev. Biol. 134, 289–315.

Butler, A., Hoffman, P., Smibert, P., Papalexi, E., Satija, R., 2018. Integrating single-cell transcriptomic data across different conditions, technologies, and species. Nat. Biotechnol. 36 (5), 411–420.

Chakraborty, R., Saddouk, F.Z., Carrao, A.C., Krause, D.S., Greif, D.M., Martin, K.A., 2019. Promoters to study vascular smooth muscle. Arterioscler. Thromb. Vasc. Biol. 39, 603–612.

Chen, S., Birk, D.E., 2013. The regulatory roles of small leucine-rich proteoglycans in extracellular matrix assembly. FEBS J. 280, 2120–2137.

Cohn, M.J., 2021. GUDMAP Consortium. https://doi.org/10.25548/17-DSBR.

Creff, J., Besson, A., 2020. Functional versatility of the CDK inhibitor p57(Kip2). Front Cell Dev Biol 8, 584590.

Denayer, S., Helsen, C., Thorrez, L., Haelens, A., Claessens, F., 2010. The rules of DNA recognition by the androgen receptor. Mol. Endocrinol. 24, 898–913.

Edgar, R., Domrachev, M., Lash, A.E., 2002. Gene Expression Omnibus: NCBI gene expression and hybridization array data repository. Nucleic Acids Res. 30, 207–210.

Gandhi, D., Molotkov, A., Batourina, E., Schneider, K., Dan, H., Reiley, M., Laufer, E., Metzger, D., Liang, F., Liao, Y., Sun, T.T., Aronow, B., Rosen, R., Mauney, J., Adam, R., Rosselot, C., Van Batavia, J., McMahon, A., McMahon, J., Guo, J.J., Mendelsohn, C., 2013. Retinoid signaling in progenitors controls specification and regeneration of the urothelium. Dev. Cell 26, 469–482.

Georgas, K.M., Armstrong, J., Keast, J.R., Larkins, C.E., McHugh, K.M., Southard-Smith, E.M., Cohn, M.J., Batourina, E., Dan, H., Schneider, K., Buehler, D.P., Wiese, C.B., Brennan, J., Davies, J.A., Harding, S.D., Baldock, R.A., Little, M.H., Vezina, C.M., Mendelsohn, C., 2015. An illustrated anatomical ontology of the developing mouse lower urogenital tract. Development 142, 1893–1908.

Glucksmann, A., Ooka-Souda, S., Miura-Yasugi, E., Mizuno, T., 1976. The effect of neonatal treatment of male mice with antiandrogens and of females with androgens on the development of the os penis and os clitoridis. J. Anat. 121, 363–370.

Goldstein, J.L., Wilson, J.D., 1975. Genetic and hormonal control of male sexual differentiation. J. Cell. Physiol. 85, 365–377.

Gomez, D., Swiatlowska, P., Owens, G.K., 2015. Epigenetic control of smooth muscle cell identity and lineage memory. Arterioscler. Thromb. Vasc. Biol. 35, 2508–2516.

Gredler, M.L., Larkins, C.E., Leal, F., Lewis, A.K., Herrera, A.M., Perriton, C.L., Sanger, T.J., Cohn, M.J., 2014. Evolution of external genitalia: insights from reptilian development. Sex Dev 8, 311–326.

Gredler, M.L., Patterson, S.E., Seifert, A.W., Cohn, M.J., 2020. Foxa1 and Foxa2 orchestrate development of the urethral tube and division of the embryonic cloaca through an autoregulatory loop with Shh. Dev. Biol. 465, 23–30.

Gredler, M.L., Sanger, T.J., Cohn, M.J., 2015a. Development of the cloaca, hemipenes, and hemiclitores in the green anole, Anolis carolinensis. Sex Dev 9, 21–33.

Gredler, M.L., Seifert, A.W., Cohn, M.J., 2015b. Morphogenesis and patterning of the phallus and cloaca in the American alligator, alligator mississippiensis. Sex Dev 9, 53–67.

Gredler, M.L., Seifert, A.W., Cohn, M.J., 2015c. Tissue-specific roles of Fgfr2 in development of the external genitalia. Development 142, 2203–2212.

Guillette Jr., L.J., Pickford, D.B., Crain, D.A., Rooney, A.A., Percival, H.F., 1996. Reduction in penis size and plasma testosterone concentrations in juvenile alligators living in a contaminated environment. Gen. Comp. Endocrinol. 101, 32–42.

Haller, M., Ma, L., 2019. Temporal, spatial, and genetic regulation of external genitalia development. Differentiation; research in biological diversity 110, 1–7.

Haraguchi, R., Mo, R., Hui, C., Motoyama, J., Makino, S., Shiroishi, T., Gaffield, W., Yamada, G., 2001. Unique functions of Sonic hedgehog signaling during external genitalia development. Development 128, 4241–4250.

Hashimoto, D., Hyuga, T., Acebedo, A.R., Alcantara, M.C., Suzuki, K., Yamada, G., 2019. Developmental mutant mouse models for external genitalia formation. Congenital. Anom. 59, 74–80.

Herrera, A.M., Brennan, P.L., Cohn, M.J., 2015. Development of avian external genitalia: interspecific differences and sexual differentiation of the male and female phallus. Sex Dev 9, 43–52.

Herrera, A.M., Cohn, M.J., 2014. Embryonic origin and compartmental organization of the external genitalia. Sci. Rep. 4, 6896.

Hutson, J.M., Grover, S.R., O'Connell, M., Pennell, S.D., 2014. Malformation syndromes associated with disorders of sex development. Nat. Rev. Endocrinol. 10, 476–487.

Hynes, P.J., Fraher, J.P., 2004a. The development of the male genitourinary system: II. The origin and formation of the urethral plate. Br. J. Plast. Surg. 57, 112–121.

Hynes, P.J., Fraher, J.P., 2004b. The development of the male genitourinary system: III. The formation of the spongiose and glandar urethra. Br. J. Plast. Surg. 57, 203–214.

Kawabata, Y., Kamio, A., Jincho, Y., Sakashita, A., Takashima, T., Kobayashi, H., Matsui, Y., Kono, T., 2019. Sex-specific histone modifications in mouse fetal and neonatal germ cells. Epigenomics 11, 543–561.

Kurita, T., 2010. Developmental origin of vaginal epithelium. Differentiation; research in biological diversity 80, 99–105.

Larkins, C.E., Cohn, M.J., 2015. Phallus development in the turtle Trachemys scripta. Sex Dev 9, 34–42.

Leal, F., Cohn, M.J., 2015. Development of hemipenes in the ball python snake Python regius. Sex Dev 9, 6–20.

Lee, C., Huang, C.H., 2013. LASAGNA-Search: an integrated web tool for transcription factor binding site search and visualization. Biotechniques 54, 141–153.

Lin, C., Yin, Y., Bell, S.M., Veith, G.M., Chen, H., Huh, S.H., Ornitz, D.M., Ma, L., 2013. Delineating a conserved genetic cassette promoting outgrowth of body appendages. PLoS Genet. 9, e1003231.

Love, M.I., Huber, W., Anders, S., 2014. Moderated estimation of fold change and dispersion for RNA-seq data with DESeq2. Genome Biol. 15, 550.

Lyon, M.F., Hawkes, S.G., 1970. X-linked gene for testicular feminization in the mouse. Nature 227, 1217–1219.

Matsumaru, D., Haraguchi, R., Moon, A.M., Satoh, Y., Nakagata, N., Yamamura, K., Takahashi, N., Kitazawa, S., Yamada, G., 2014. Genetic analysis of the role of Alx4 in the coordination of lower body and external genitalia formation. Eur. J. Hum. Genet. 22, 350–357.

Mierzejewska, K., Borkowska, S., Suszynska, E., Suszynska, M., Poniewierska-Baran, A., Maj, M., Pedziwiatr, D., Adamiak, M., Abdel-Latif, A., Kakar, S.S., Ratajczak, J., Kucia, M., Ratajczak, M.Z., 2015. Hematopoietic stem/progenitor cells express several functional sex hormone receptors-novel evidence for a potential developmental link between hematopoiesis and primordial germ cells. Stem Cell. Dev. 24, 927–937.

Mohammed, M., Bright, F., Mteta, A., Mbwambo, J., Ngowi, B.N., Mbwambo, O., Yongolo, S., Mganga, A., 2020. Long-term complications of hypospadias repair: a ten-year experience from northern zone of Tanzania. Res. Rep. Urol. 12, 463–469.

Morgan, E.A., 2003. Loss of Bmp7 and Fgf8 signaling in Hoxa13-mutant mice causes hypospadia. Development 130, 3095–3109.

Murakami, R., 1987. A histological study of the development of the penis of wild-type and androgen-insensitive mice. J. Anat. 153, 223–231.

Murakami, R., Mizuno, T., 1986. Proximal-distal sequence of development of the skeletal tissues in the penis of rat and the inductive effect of epithelium. J. Embryol. Exp. Morphol. 92, 133–143.

Nelson, C.P., Park, J.M., Wan, J., Bloom, D.A., Dunn, R.L., Wei, J.T., 2005. The increasing incidence of congenital penile anomalies in the United States. J. Urol. 174, 1573–1576.

O'Shaughnessy, P.J., Baker, P., Sohnius, U., Haavisto, A.-M., Charlton, H.M., Huhtaniemi, I., 1998. Fetal development of Leydig cell activity in the mouse is independent of pituitary gonadotroph function. Endocrinology 139, 1141–1146.

Perriton, C.L., Powles, N., Chiang, C., Maconochie, M.K., Cohn, M.J., 2002. Sonic hedgehog signaling from the urethral epithelium controls external genital development. Dev. Biol. 247, 26–46.

Phillips, T.R., Wright, D.K., Gradie, P.E., Johnston, L.A., Pask, A.J., 2015. A comprehensive atlas of the adult mouse penis. Sexual Development 9, 162–172.

Pollen, A.A., Nowakowski, T.J., Shuga, J., Wang, X., Leyrat, A.A., Lui, J.H., Li, N., Szpankowski, L., Fowler, B., Chen, P., Ramalingam, N., Sun, G., Thu, M., Norris, M., Lebofsky, R., Toppani, D., Kemp 2nd, D.W., Wong, M., Clerkson, B., Jones, B.N., Wu, S., Knutsson, L., Alvarado, B., Wang, J., Weaver, L.S., May, A.P., Jones, R.C., Unger, M.A., Kriegstein, A.R., West, J.A., 2014. Low-coverage single-cell mRNA sequencing reveals cellular heterogeneity and activated signaling pathways in developing cerebral cortex. Nat. Biotechnol. 32, 1053–1058.

Rosset, E.M., Bradshaw, A.D., 2016. SPARC/osteonectin in mineralized tissue. Matrix Biol. 52–54, 78–87.

Ru, W., Tang, D., Wu, D., Tao, C., Chen, G., Wei, J., Tian, H., Shu, Q., 2021. Identification of risk factors associated with numerous reoperations following primary hypospadias repair. J. Pediatr. Urol. 17, 61.e1–61.e5.

Sanger, T.J., Gredler, M.L., Cohn, M.J., 2015. Resurrecting embryos of the tuatara, Sphenodon punctatus, to resolve vertebrate phallus evolution. Biol. Lett. 11, 20150694..

Satija, R., Farrell, J.A., Gennert, D., Schier, A.F., Regev, A., 2015. Spatial reconstruction of single-cell gene expression data. Nat. Biotechnol. 33 (5), 495–502.

Seifert, A.W., Harfe, B.D., Cohn, M.J., 2008. Cell lineage analysis demonstrates an endodermal origin of the distal urethra and perineum. Dev. Biol. 318, 143–152.

Shaffer, P.L., Jivan, A., Dollins, D.E., Claessens, F., Gewirth, D.T., 2004. Structural basis of androgen receptor binding to selective androgen response elements. Proc. Natl. Acad. Sci. U. S. A. 101, 4758–4763.

Springer, A., van den Heijkant, M., Baumann, S., 2016. Worldwide prevalence of hypospadias. J. Pediatr. Urol. 12 (3), 152. e151–157.

Stewart, M.K., Mattiske, D.M., Pask, A.J., 2018. In utero exposure to both high- and low-dose diethylstilbestrol disrupts mouse genital tubercle development. Biol. Reprod. 99, 1184–1193.

Su, T., Liu, H., Zhang, D., Xu, G., Liu, J., Evans, S.M., Pan, J., Cui, S., 2019. LIM homeodomain transcription factor Isl1 affects urethral epithelium differentiation and apoptosis via Shh. Cell Death Dis. 10, 713.

Suzuki, K., Haraguchi, R., Ogata, T., Barbieri, O., Alegria, O., Vieux-Rochas, M., Nakagata, N., Ito, M., Mills, A.A., Kurita, T., Levi, G., Yamada, G., 2008. Abnormal urethra formation in mouse models of split-hand/split-foot malformation type 1 and type 4. Eur. J. Hum. Genet. 16, 36–44.

Suzuki, K., Ogino, Y., Murakami, R., Satoh, Y., Bachiller, D., Yamada, G., 2002. Embryonic development of mouse external genitalia: insights into a unique mode of organogenesis. Evol. Dev. 4, 133–141.

Taneli, C., Tanriverdi, H.I., Genc, A., Sencan, A., Gunsar, C., Yilmaz, O., 2021. Tubularized reconstructed plate urethroplasty: an alternative technique for distal hypospadias repair. Urology 148, 243–249.

Tschopp, P., Sherratt, E., Sanger, T.J., Groner, A.C., Aspiras, A.C., Hu, J.K., Pourquie, O., Gros, J., Tabin, C.J., 2014. A relative shift in cloacal location repositions external genitalia in amniote evolution. Nature 516, 391–394.

Wang, C., Wang, J., Borer, J.G., Li, X., 2013. Embryonic origin and remodeling of the urinary and digestive outlets. PloS One 8, e55587.

Wang, W., Wan, L., Chen, Z., Jin, X., Li, D., 2020. Myofibroblasts control the proliferation of fetal hepatoblasts and their differentiated cholangiocytes during the hepatoblast-to-cholangiocyte transition. Biochem. Biophys. Res. Commun. 522, 845–851.

Williams-Ashman, H.G., Reddi, A.H., 1991. Differentiation of mesenchymal tissues during phallic morphogenesis with emphasis on the os penis: roles of androgens and other regulatory agents. J. Steroid Biochem. Mol. Biol. 39, 873–881.

Yang, J.H., Menshenina, J., Cunha, G.R., Place, N., Baskin, L.S., 2010. Morphology of mouse external genitalia: implications for a role of estrogen in sexual dimorphism of the mouse genital tubercle. J. Urol. 184, 1604–1609.

Yang, Y., Wilson, M., 2019. Genome-wide analysis of H3K4me3 and H3K27me3 modifications throughout the mouse urogenital ridge at E11.5. Gene Reports 16, 100412.

Zheng, Z., Armfield, B.A., Cohn, M.J., 2015. Timing of androgen receptor disruption and estrogen exposure underlies a spectrum of congenital penile anomalies. Proc. Natl. Acad. Sci. U. S. A. 112 (52), E7194–E7203.